Transient Stability Assessment and Enhancement of Grid-Forming Converters Embedding Current Reference Saturation as Current Limiting Strategy

Ebrahim Rokrok, *Student Member, IEEE,* Taoufik Qoria, Antoine Bruyere, *Member, IEEE,* Bruno Francois, *Senior Member, IEEE* and Xavier Guillaud, *Member, IEEE*

***Abstract*—This paper deals with the transient stability of a grid-forming converter while embedding a current reference saturation strategy. The novelty of this work consists in investigating the impact of the current reference angle on the transient stability. In case of a voltage sag, analytical formulas to forecast the critical clearing angle (CCA) and critical clearing time (CCT) while considering different values of the current reference angle are derived. It has been demonstrated that the choice of this angle is constrained by the ability of the VSC to switch back to the voltage control mode. Based on that, its optimal value that enhances the transient stability and allows a switching from the current control mode to the voltage control mode is designed. Thereafter, the effectiveness of this optimal choice to guarantee the stability in case of a phase shift caused by a line re-closing event has been confirmed. Time-domain simulations are performed in Matlab-Simulink environment to validate the correctness of the theoretical approaches.**

***Index Terms*—Critical clearing time, current limitation, current saturation algorithm, grid-forming control, inertial effect, transient stability.**

I. Introduction

THE energy paradigms have experienced a significant change from fossil-based to clean renewables in the past few decades. The scenario of highly penetrated renewables is going to be further enhanced. Hence, more power electronic converters are integrated in electrical grids to connect the renewable energy source and to transmit this power with high-voltage direct current (HVDC) lines [1]. When the synchronous generators (SGs) are dominating the electrical grid, they can create a stable voltage and frequency that enable the power converters to be synchronized at the point of common coupling (PCC) through a phase-locked loop (PLL) and then to inject the power to the grid. These converters are known as "grid-following" converters. Increasing the grid-following converters will strongly affect the power system stability and security [2]–[4].

To tackle these challenges, the way to control power converters has to be changed from grid-following control to grid-forming control in which the converter behaves as a voltage source. Due to the voltage source behavior of a grid-forming converter, the overcurrent protection requires a specific attention [5]. Compared to synchronous generators (SGs) that can support up to seven times over their rated current, power converters can only cope with few percent of overcurrent (typically 20%) [6]. Therefore, the grid-forming converters have to be protected against extreme faults such as short circuit, heavy load connection, line-tripping/reclosing and voltage phase jump only based on the control, while being able to stay synchronized to the power system.

Many control strategies have been proposed for grid-forming converters in order to limit the current during large transients. One strategy is to limit the current with a current saturation algorithm (CSA). In practice, this technique is implemented on the converters with cascaded inner voltage and current control loops in which the generated current reference is saturated during over current [7]. Another well-known current limiting strategy is based on a virtual impedance (VI) that emulates the effect of an impedance when the current exceeds its nominal value [6], [8], [9]. This method has shown its effectiveness to limit the current transients in case of various events while keeping the voltage source nature of the power converter. In [10] a comparative study between the CSA and VI strategies in case of a three-phase short circuit is performed. It has been demonstrated that the CSA strategy has a better performance in limiting the current during the first milliseconds after the fault, while for the VI strategy, some overcurrent during the first 25 milliseconds have been observed.

Grid-forming converters have not only to cope with the current limitation, but also to remain stable and synchronized to the AC grid after large disturbances. In the power system, this ability is defined as the angle stability or the transient stability. Regarding this aspect, it has been studied in [11], [12] while neglecting the current limitation. However, as mentioned in [7], [10], the current limitation has a large impact on the transient stability. In [13], [14], the transient stability of the grid-forming converters including the VI is investigated. In [13], the transient stability of a droop-based virtual synchronous generator in case of a 30% grid voltage sag is studied in two steps. First, the VI is not taken into account. Based on that, a theoretical approach relying on the Lyapunov's direct method to predict the critical clearing time (CCT) is developed. Then, when including a constant VI, it has been demonstrated that the stability region becomes more limited. In [14], a method for critical clearing angle (CCA) and CCT calculation in case of a bolted fault while

Ebrahim Rokrok, Taoufik Qoria, Antoine Bruyere, Bruno Francois and Xavier Guillaud are with L2EP, Univ. Lille, Arts et Metiers Institute of Technology, Centrale Lille, Yncrea Hauts-de-France, ULR 2697 - L2EP – Laboratoire d'Electrotechnique et d'Electronique de Puissance, F-59000 Lille, France.

limiting the current with a VI is proposed. To improve the CCA and CCT, authors in [13], [14] propose to decrease the power reference with respect to the AC voltage magnitude. An alternative solution that consists to increase the inertia constant with respect to the AC voltage magnitude [15] is suggested. Referring to [16], the management of the power reference or inertia constant with respect to the voltage magnitude is mainly effective when the voltage magnitude is decreasing as in case of a voltage sag. However, in the case of a phase shift, which is a very likely event, these solutions are useless.

Considering the effect of a CSA on the transient stability, authors in [7], [17] have determined a stability criterion based on CCA for an inertia-less droop-controlled VSC in case of a voltage sag. Then, in [7] a stability enhanced P-f droop control scheme is presented to improve the transient stability of the VSC by modifying the frequency setpoint through the quadrature voltage axis. In [7], [17], a very strong assumption is made while analyzing the transient stability, where the current reference priority has been given to the d-axis component, so as the converter injects the active current during the fault. To the best of our knowledge, the impact of the current reference priority (i.e., the current reference angle) has not been justified and its impact on the transient stability has not been highlighted. Based on that, this paper proposes the main contributions:

- Investigation of the impact of the current reference angle on the transient stability by means of analytical formulas of CCA and CCT.
- Proposal of an optimum design of the saturated current angle, which is based on a trade-off between the transient stability enhancement and the ability to switch-back to the voltage control mode after the fault clearance.

The effectiveness of the design of the saturated current angle is demonstrated for two different types of balanced faults (i.e., three phase short-circuit fault and phase-shift).

The remaining of the paper is organized as follows. Section II introduces the studied system including the grid-forming control architecture and large signal models for transient stability analysis. In section III, the transient stability of the grid-forming converter in the case of a voltage is assessed and enhanced. Section IV demonstrates the effectiveness of the proposed method in increasing the stability margin of the system in case of a phase shift. Finally, section V concludes the paper.

II. Presentation of the Studied System

The main aim of a Voltage Source Converter (VSC) is to convert a DC power to AC power and vice-versa. In what follows, the VSC is considered as a controllable three-phase AC voltage source: v_{m_a}, v_{m_b}, v_{m_c}, which are modulated from a constant DC bus voltage (see Fig. 1). The control system defines a set of three-phase reference signals $v^*_{m_a}$, $v^*_{m_b}$, $v^*_{m_c}$ in such a way that the average values of v_{m_a}, v_{m_b}, v_{m_c} during the PWM period are equal to $v^*_{m_a}$, $v^*_{m_b}$, $v^*_{m_c}$. Following assumptions are considered:

- It is supposed that the VSC is connected to the grid with a transformer, which is modeled with its series impedance (R_c, L_c).

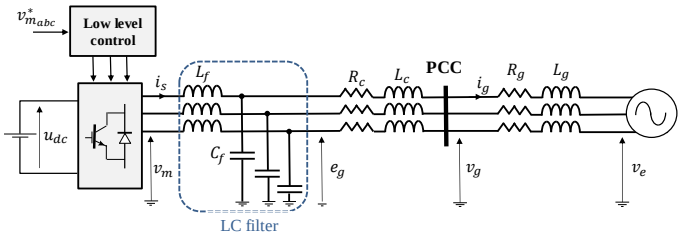

Fig. 1. Generic topology of the VSC.

- An LC filter $(L_f C_f)$ is used to eliminate the high-frequency harmonics caused by the PWM signals.
- The converter is connected to a power transmission system, and therefore, the resistance is much smaller than the reactance.
- The grid is modeled by a Thevenin equivalent circuit composed of a voltage source $v_{e_{abc}}$, an inductance L_g and a resistance R_g.
- The converter is connected to a power transmission system, and therefore, the resistance is much smaller than the reactance ($R_g << L_g$).

A. Control Structure

The control structure of the grid-forming VSC is presented in Fig. 2. Inner control includes the cascaded voltage and current control loops, which allows the output voltage e_g to track its reference value e^*_g. The voltage e_g is aligned to the d-axis ($e^*_{gq} = 0\ pu$).

In this paper, the outer active power controller is based on a PLL-free IP-controller [15]:

$$\omega_g = \frac{1}{2Hs}(P_0 - P) - k_p P, \tag{1}$$

$$\theta_g = \omega_g \omega_b / s, \tag{2}$$

where H, k_p and P_0 denote the inertia constant, damping factor and active power setpoint, respectively. θ_g denotes the time-domain internal angle.

Generally, the dynamic of the outer power loop is over ten times slower than that of the inner control loops [18]. In fact, when analyzing the transient stability problem caused by the power control loop, the inner control loops can be neglected because of their faster response time [7], [11]. Hence, based on this assumption, large signal models for transient stability studies are derived.

B. Phasor Model for Transient Stability Studies

In order to analyze the large transient stability, a classical steady state model is proposed in Fig. 3 (a). Neglecting the internal loops dynamics, only the voltage e_g is considered in the converter side. In steady state, it is represented by a complex quantity $\bar{E}_g$. The magnitude is supposed to be 1 pu and the angle is δ_g, which is linked with $\theta_g : \theta_g = \omega_g t + \delta_g$. $\bar{V}_e$ represents the voltage on the grid side, the magnitude is 1 pu and the phase is δ_e. By neglecting the resistance, the well-known expression of the power can be written as follows:

$$P = \frac{E_g V_e}{X_c + X_g} \sin(\delta_g - \delta_e) = P_{\max} \sin(\delta), \tag{3}$$

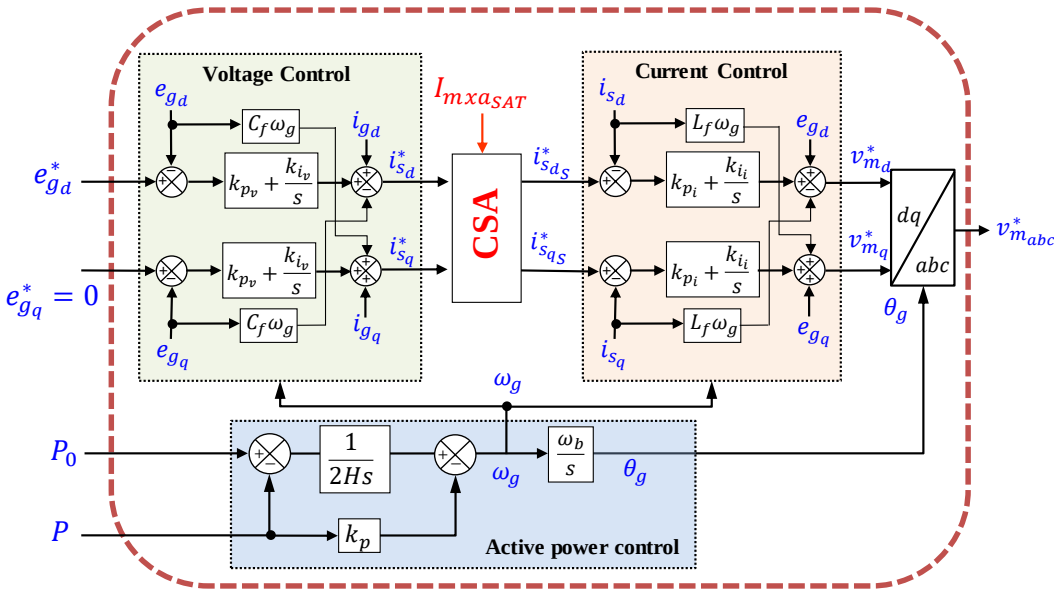

Fig. 2. General configuration of the implemented VSC control structure.

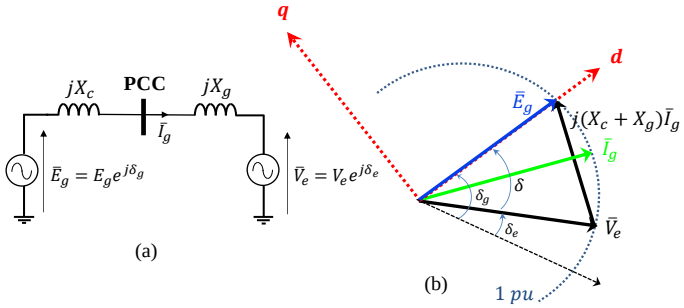

Fig. 3. (a) Equivalent circuit of the VSC. (b) Phasor-diagram.

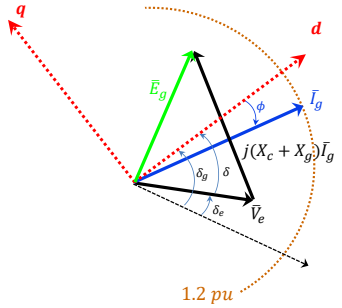

Fig. 4. Phasor-diagram of the VSC in saturated operation mode.

where $\delta = \delta_g - \delta_e$ denotes the power angle and $P_{max} = E_g V_e/(X_c + X_g)$.

Fig. 3 (b) illustrates the phasor diagram associated to this system in unsaturated operation mode. The vector $\bar{E}_g$ (in blue) is the control vector that is supposed to be aligned with the d-axis. The vector of the current $\bar{I}_g$ (in green) is a consequence of this operation mode.

During some transient times, the current may increase over the maximum current of the converter. To limit the current, a CSA is used and defined as follows [10], [15]:

$$\begin{cases} i^*_{s_{dS}} = i^*_{s_d}, \quad i^*_{s_{dS}} = i^*_{s_d} & if \quad \sqrt{i^2_{s_d} + i^2_{s_q}} \leqslant I_{\max_{SAT}} \\ i^*_{s_{dS}} = I_{\max_{SAT}} \cos(-\phi) & if \quad \sqrt{i^2_{s_d} + i^2_{s_q}} > I_{\max_{SAT}} \\ i^*_{s_{qS}} = I_{\max_{SAT}} \sin(-\phi) & \end{cases} \tag{4}$$

$I_{max_{SAT}}$ stands for the maximum allowable current magnitude of the converter, which is typically 1.2 (pu). $i^*_{s_{dqS}}$ denotes the saturated d-q currents. By neglecting the current in the capacitor, it is possible to draw a new phasor diagram of the VSC (Fig. 4). The magnitude of $\bar{I}_g$ is $I_{max_{SAT}}$, its angle ϕ can be chosen freely by the control. It is referenced to the d axis. $\bar{E}_g$ is a consequence in this operation mode, it is not aligned any more with the d-axis.

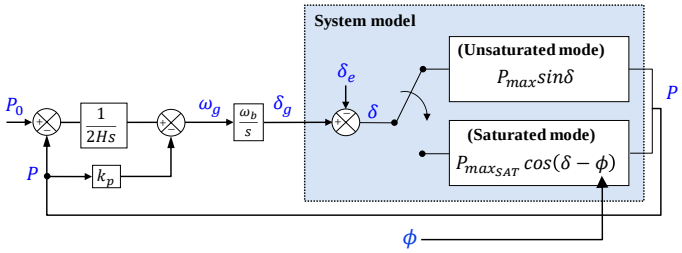

Fig. 5. Large signal model of the grid-forming converter.

The active power in saturated operation mode is calculated with the grid voltage $\bar{V}_e$ and the control vector $\bar{I}_g$ as follows [7], [17]:

$$P = V_e I_{\max_{SAT}} \cos(\delta_e - (\delta_g - \phi)) = P_{\max_{SAT}} \cos(\delta - \phi), \tag{5}$$

where $P_{max_{SAT}} = V_e I_{max_{SAT}}$. According to (3) and (5), the large signal model of the grid-forming converter for both saturated and unsaturated operation modes is illustrated in Fig. 5.

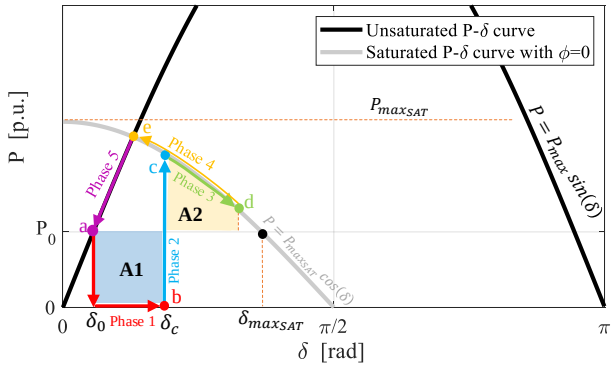

Fig. 6. Operation mechanism of the VSC under 100% voltage sag.

In the literature, the angle ϕ has been set to $\phi = 0$ rad [7], [14], [17]. However, this choice has not been justified and its impact on the stability has not been seen. In this paper, the effect of this choice on the transient stability of the grid-forming converter under various events is investigated.

III. Transient Stability Analysis in Case of a Voltage Sag

In this section, the transient stability of the grid-forming converter in case of a 100% voltage sag at the PCC is studied. The quasi-static $P-\delta$ characteristic of the grid-forming converter for both saturated and unsaturated operation mode is used to study the large signal stability graphically and to propose an analytical formula to calculate the critical clearing time.

A. Operation Mechanism Under A 100% Voltage Sag

Fig. 6 describes the operation mechanism of the grid-forming VSC subjected to a bolted fault. Initially the converter is operating in normal condition and the initial operating point is (δ_0, P_0):

- Phase 1: The voltage drops to zero resulting in an increase of the current, which is limited by the CSA, and a decrease of the active power. According to the control described in Fig. 5, the angle δ increases untill δ_c, which is defined as the clearing angle (moving from 'a' to 'b').
- Phase 2: The fault is cleared, the CSA remains activated and the operating point jumps to the point (c) located on the saturated $P-\delta$ curve.
- Phase 3: The active power is higher than its setpoint, however, the angle δ is still increasing untill the point (d) due to the inertial effect.
- Phase 4: Once the converter frequency becomes lower than the grid frequency, the angle starts to decrease untill reaching the operating point (e), which is the intersection point of the saturated and unsaturated $P-\delta$ curves.
- Phase 5: At the operating point (e), the CSA is deactivated and the system switches back to the voltage control mode. The angle decreased in unsaturated mode until the equilibrium point (a), where $P = P_0$.

For a given δ_c, the system remains stable as long as the areas A1 and A2 are equal. The stability limit is reached when $\delta_c = \delta_{cc}$, which is called the "critical clearing angle (CCA)" δ_{cc}. Under this condition, the internal angle reaches to its maximum value $\delta_{max_{SAT}}$ after the fault clearance.

$$\delta_{\max_{SAT}} = a\cos(\frac{P_0}{P_{\max_{SAT}}}). \tag{6}$$

TABLE I
System and Control Parameters

Symbol	Quantity	Symbol	Quantity
$P_b = S_b$	1000 MW	U_{ac}	320 kV
$L_g = 10R_g$	0.1 pu	$I_{max_{SAT}}$	1.2 pu
L_c	0.15 pu	$e^*_{g_d}$	1 pu
R_c	0.005 pu	$e^*_{g_q}$	0 pu
C_f	0.066 pu	k_{p_i}	0.73 pu
L_f	0.15 pu	k_{i_i}	1.19 pu
R_f	0.005 pu	k_{p_v}	0.52 pu
V_e	1 pu	k_{i_v}	1.16 pu
ω_b	314.16 rad/s	H	5 s
U_{dc}	640 kV	k_p	0.007

B. Critical Clearing Time Calculation

The critical clearing angle is calculated by considering equal surfaces A1 and A2:

$$\int_{\delta_0}^{\delta_{cc}} P_0 d\delta = \int_{\delta_{cc}}^{\delta_{\max_{SAT}}} (P_{\max_{SAT}}\cos(\delta) - P_0)d\delta$$
$$\rightarrow \delta_{cc} = a\sin(\frac{P_0(\delta_0 - \delta_{\max_{SAT}})}{P_{\max_{SAT}}} + \sin(\delta_{\max_{SAT}})), \tag{7}$$

where $\delta_0 = a\sin(\frac{P_0(X_c+X_g)}{E_g V_c})$. In order to calculate the critical clearing time (CCT) t_{cc}, the expression of the angle δ during the phase 1 is needed. According to the control presented in Fig. 5, it can be written:

$$\delta(t) = \frac{\omega_b P_0}{4H}t^2 + \delta_0 \ . \qquad (\delta_0 \leqslant \delta \leqslant \delta_{cc}) \tag{8}$$

Hence, the CCT can be expressed as:

$$t_{cc} = 2(\sqrt{\frac{H(\delta_{cc} - \delta_0)}{\omega_b P_0}}). \tag{9}$$

Equation (9) clearly demonstrates the effect of the initial operating point and inertial effect on the CCT. Two large assumptions have been used to obtain the expression of the critical clearing time:
1- The effect of the damping is negligible.
2- The quasi static model is valid enough even during large transient phenomena.
The validity of these assumptions is demonstrated in the following lines through dynamic simulations.

The system and control parameters are given in the Table I. Note that an anti-windup strategy is adopted to the PI regulators in the voltage loop [16]. Considering the given parameters in Table I, the CCT predicted from (9) and the one observed from the time-domain simulations are compared in Table II for different operating points. One can notice a small error between both CCTs. This error is due to the damping effect as it is mentioned in [19].

Taking $P_0 = 1$ [pu] as an illustrative example, Fig 7 shows the simulation results with two different fault durations

TABLE II
RESULTS OF THE CCT DETERMINATION

	$\phi = 0$	
P_0	Predicted CCT by (9)	CCT in simulation
1 pu	41 ms	38 ms
0.9 pu	69 ms	63 ms
0.8 pu	99 ms	91 ms
0.7 pu	133 ms	120 ms
0.6 pu	173 ms	157 ms
0.5 pu	221 ms	204 ms

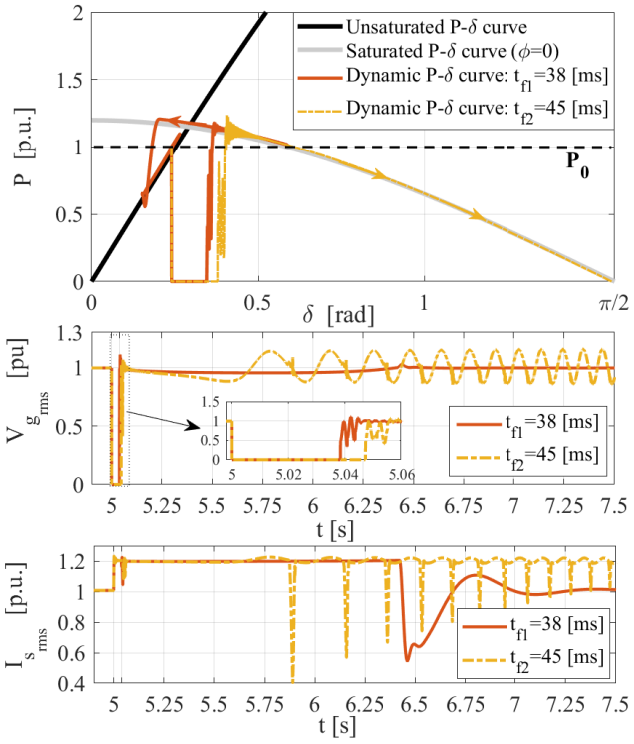

Fig. 7. Simulation results in case of a 100% voltage sag with different fault time durations.

of $t_{f1} = t_{cc} = 38$ [ms] and $t_{f2} > t_{cc}$ (45 [ms]). As expected if the clearing time is lower or equal to the CCT, the internal angle of the VSC stably recovers its equilibrium point, otherwise it diverges and the system loses the synchronism.

In any case, the obtained value of the critical clearing time is quite small. The next section proposes a solution based on the current reference angle to increase this critical clearing time.

C. Impact of the Saturated Current Angle ϕ on Transient Stability

The obtained value of the critical clearing time is quite small. With reference to (9), two control parameters that are the power setpoint (P_0) and inertia constant (H) affect the transient stability of the VSC. As pointed out in [13] the transient stability of grid-forming converters can be enhanced by reducing the active power reference during grid voltage sags. References [14], [15] have demonstrated that increasing the inertia constant in case of voltage sag also improves the transient stability. The angle ϕ is a new control degree of

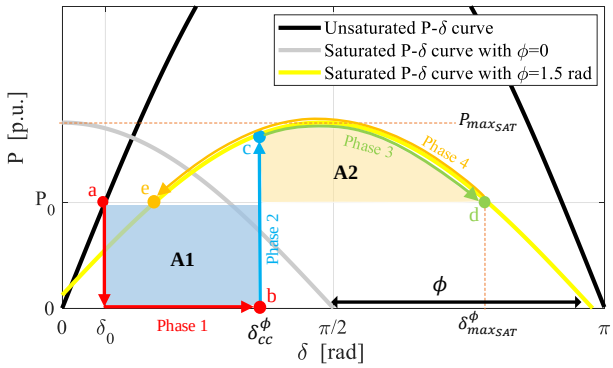

Fig. 8. Operation mechanism of the VSC under a 100% voltage sag by considering $\phi = 1.5$ rad.

freedom that has not been exploited in the literature to enhance the transient stability of the grid-forming VSCs.

As explained in (5), the angle ϕ has an influence on the expression of the active power. When applying a positive angle, the quasi-static $P-\delta$ curve in saturated operation mode is shifted to the right side (see Fig. 8). In this condition, the maximum angle that the converter can reach is given by:

$$\delta^{\phi}_{\max_{SAT}} = a\cos\left(\frac{P_0}{P_{\max_{SAT}}}\right) + \phi. \tag{10}$$

Using EAC in this condition, the following expression for the CCA and CCT are obtained:

$$\delta^{\phi}_{cc} = a\sin\left(\frac{P_0(\delta_0 - \delta^{\phi}_{\max_{SAT}})}{P_{\max_{SAT}}} + \sin(\delta^{\phi}_{\max_{SAT}} - \phi)\right) + \phi, \tag{11}$$

$$t^{\phi}_{cc} = 2\left(\sqrt{\frac{H(\delta^{\phi}_{cc} - \delta_0)}{\omega_b P_0}}\right). \tag{12}$$

Comparing to (7) and (9), (11) and (12) demonstrate that the CCA and CCT are increased with respect to the increase of ϕ giving more time to disconnect the disturbance while ensuring a stable restoration. However, the parameter ϕ could not be incautiously chosen. Actually, referring to Fig. 8, and focusing on the "Phase 4", where the operating point moves from (d) to (e). In this particular situation, the internal angle is locked in the operating point (e) located in the saturated $P-\delta$ curve since P reaches P_0. In other word, the system cannot switch back to the voltage control mode. Therefore, the choice of ϕ is constrained by the ability of the VSC to switch from the current control mode to the voltage control mode. Consequently, ϕ_{opt} is defined as optimum shift of saturated $P-\delta$ curve that allows at once a transient stability enhancement and a post-fault recovering to the voltage control mode. The rightness of the analysis proposed in this subsection is validated through time domain simulations in the next subsection.

D. Optimal Design of the Saturated Current Angle ϕ

In order to avoid the internal angle being locked in the saturated mode during re-synchronization phase, the value of ϕ can be calculated in such a way that the operating points 'a' and 'e' in Fig. 8 are matched, which yields:

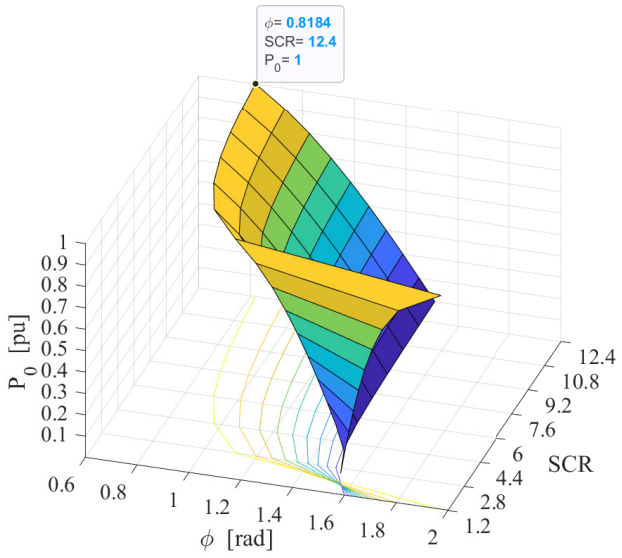

Fig. 9. The angle ϕ with respect to the variation of SCR and Power setpoint.

$$\phi = a\cos(\frac{P_0}{P_{\max_{SAT}}}) + a\sin(\frac{P_0}{P_{\max}}). \quad (13)$$

According to (13), the value of ϕ depends on the initial power setpoint and grid impedance. By defining the grid impedance based on the short circuit ratio (SCR) of the grid as: $SCR = 1/X_g$, it is possible to draw a surface that relates ϕ to the SCR and P_0 as shown in Fig. 9. It can be seen that for a wide range of SCR and various operating points, $\phi_{opt} = 0.8$ [rad] can be defined as an optimal value that guarantees a better transient stability compared to the case in which $\phi = 0$ rad and ensures a switching back to the voltage control mode after fault clearance.

Considering the given parameters in Table I and initial power setpoint of $P_0 = 1$ [pu], Fig. 10 shows the simulation results with two different values of ϕ. In case that $\phi = \phi_{opt}$, the theoretical value of CCT is $t_{cc} = 96$ [ms], which is higher than the CCT in the case of $\phi = 0$. As it can be seen, the system, switches back to the voltage mode at $t = 6.2$ [s]. If $\phi = 1.5$ [rad] ($\phi > \phi_{opt}$), the system remains stable and $P = P_0$ in steady-state. However, the angle reaches a new operating point, which is higher than the pre-fault value δ_0. Consequently the VSC remains operating in the saturated mode as shown by the curve of the current $I_{s_{rms}}$. This verifies the presented claims in subsection II.C.

Table III presents the CCT values while including the current angle shift for different power setpoints. These results confirm that the proposed method can enhance the transient stability and (12) gives a satisfactory accuracy in the anticipated CCT.

IV. Transient Stability Analysis in Case of a Phase Shift

Another large event, which can happen in the grid, is a line tripping/reclosing. Due to the large grid impedance variation, it results in a phase shift [20]. The stability of the VSC has

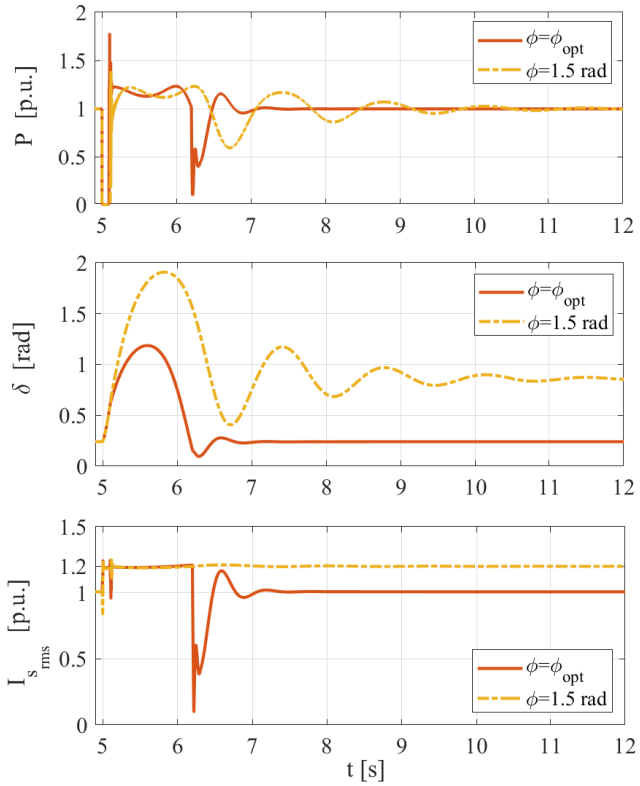

Fig. 10. Effect of including ϕ in the control on transient stability in case of a 100% voltage sag.

TABLE III
Results of the CCT determination

	$\phi = \phi_{opt}$	
P_0	Predicted CCT by (12)	CCT in simulation
1 pu	96 ms	94 ms
0.9 pu	135 ms	130 ms
0.8 pu	175 ms	164 ms
0.7 pu	217 ms	204 ms
0.6 pu	266 ms	247 ms
0.5 pu	325 ms	304 ms

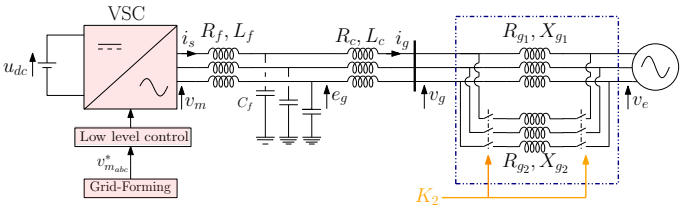

Fig. 11. Studied system with a line tripping/reclosing scenario.

to be analyzed, especially in case of a weak grid conditions. To analyze this effect, a small benchmark is studied (see Fig. 11). Depending on the K2 position, the short circuit ratio is $SCR_1 = \frac{1}{X_{g1}}$ or $SCR_2 = \frac{X_{g1}.X_{g2}}{X_{g1}+X_{g2}}$.

As previously, the different phases are described with the help of some curves derived from the quasi-static models.

Considering the line-tripping scenario, according to Fig. 12, the VSC is initially operating at the point B located on the light blue curve with $SCR = SCR_2$. When the second line is tripped, the operating point suddenly moves to the other

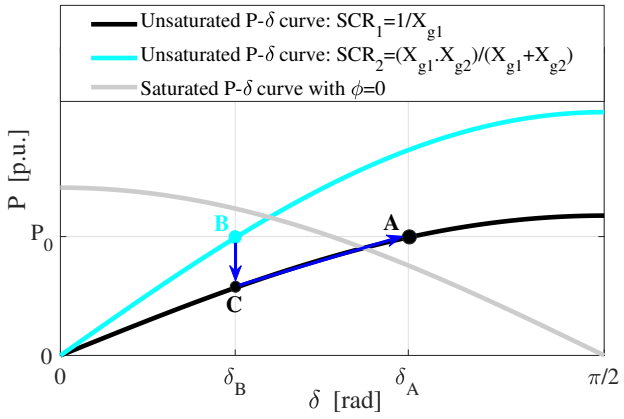

Fig. 12. Operation mechanism of the VSC in case of line tripping/reclosing under low SCR.

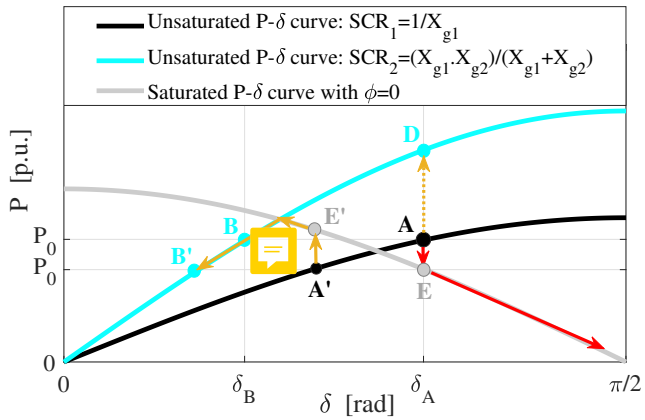

Fig. 13. Operation mechanism of the VSC in case of a line reclosing while considering a shifted saturated curve.

curve with $SCR = SCR_1$ (black curve) while keeping the same angle (point C) and then the angle increases to reach the point A where the initial operating point is recovered. It should be mentioned that in this scenario, since the active power is initially dropped and then incrementally reaches to the initial operating power, the CSA is not activated.

Considering the line-reclosing scenario, according to Fig. 13, the VSC is initially operating at the point A. At the time of connection of the second line, it is expected that the operating point jumps to the other curve with $SCR = SCR_2$ (light blue curve) while keeping the same angle (operating point D). However, reclosing the line activates the CSA and therefore, the operating point moves to the saturated curve to limit the current (operating point E). At this point, the active power is smaller than its setpoint. Therefore, the angle δ diverges and the VSC loses the synchronism. Actually, the instability issue caused by a line reclosing is linked to the location of the initial operating point with respect to the saturated curve in the$P-\delta$ plane. If the initial operating power is located above the saturated quasi-static $P-\delta$ curve, then the system loses the synchronism as explained previously. If the initial operating point is below the saturated curve (A'), the operating point moves to E', which its corresponding power is higher than the initial power setpoint. Therefore, the angle decreases to reach its new equilibrium point (B').

According to the coordinates of the initial operating point with respect to the saturated curve, the following constraints on the initial angle and therefore on the initial power setpoint can be derived to guarantees a stable line reclosing:

$$\begin{cases} P_0 \leqslant V_e I_{\max_{SAT}} \cos(\delta_0), \\ P_0 = \dfrac{E_g V_e}{X_c + \frac{1}{SCR_1}} \sin(\delta_0). \end{cases} \tag{14}$$

Therefore:

$$\delta_0 \leqslant a\tan\left(\frac{I_{\max_{SAT}}(X_c + \frac{1}{SCR_1})}{E_g}\right), \tag{15}$$

$$P_0 \leqslant \frac{E_g V_e}{X_c + \frac{1}{SCR_1}} \sin\left[a\tan\left(\frac{I_{\max_{SAT}}(X_c + \frac{1}{SCR_1})}{E_g}\right)\right]. \tag{16}$$

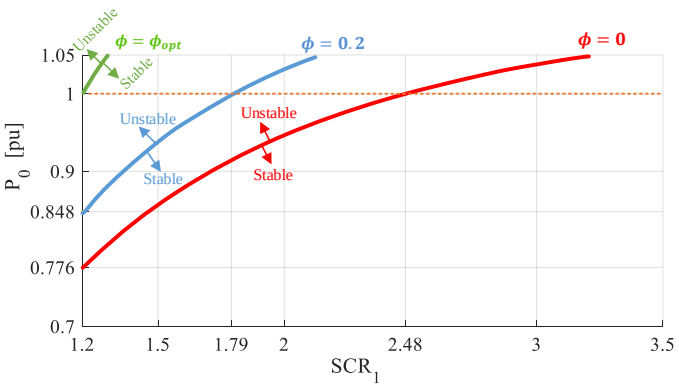

Fig. 14. Effect of shifting the saturated quasi-static $P-\delta$ curve on the stability region in case of a line-reclosing.

Using the proposed shifting of the saturated curve to the right side of the $P-\delta$ plane, (16) is updated to (17) as follows:

$$P_0 \leqslant \frac{E_g V_e}{X_c + \frac{1}{SCR_1}} \sin\left[\frac{1}{\cos\phi} a\tan\left(\frac{I_{\max_{SAT}}(X_c + \frac{1}{SCR_1})}{E_g - [I_{\max_{SAT}}(X_c + \frac{1}{SCR_1})].\sin\phi}\right)\right]. \tag{17}$$

By setting $\phi = \phi_{opt}$ in (17), Fig. 14 demonstrates the capability of the VSC to deal with the line-reclosing for the full range of initial power setpoint ($0 \leq P_0 \leq 1$) under very low grid impedances.

To verify the correctness of the presented analysis, we consider $P_0 = 1$ [pu], $SCR_1 = 1.2$, $SCR_2 = 2.4$ and simulate the line reclosing. In this situation, according to Fig. 15, if $\phi = 0$, it is expected that the VSC loses the synchronism, while if $\phi = \phi_{opt}$, it stably shifts to a new operating point. It can be seen that by using the proposed choice on the angle ϕ, the VSC can stably deal with the phase shift.

V. Conclusion

In this paper, the transient stability of the grid-forming control embedding a current saturation algorithm as the control limiting strategy has been investigated. In case of large grid disturbances, the converter switches to the current control mode. According to the active power expression in this control

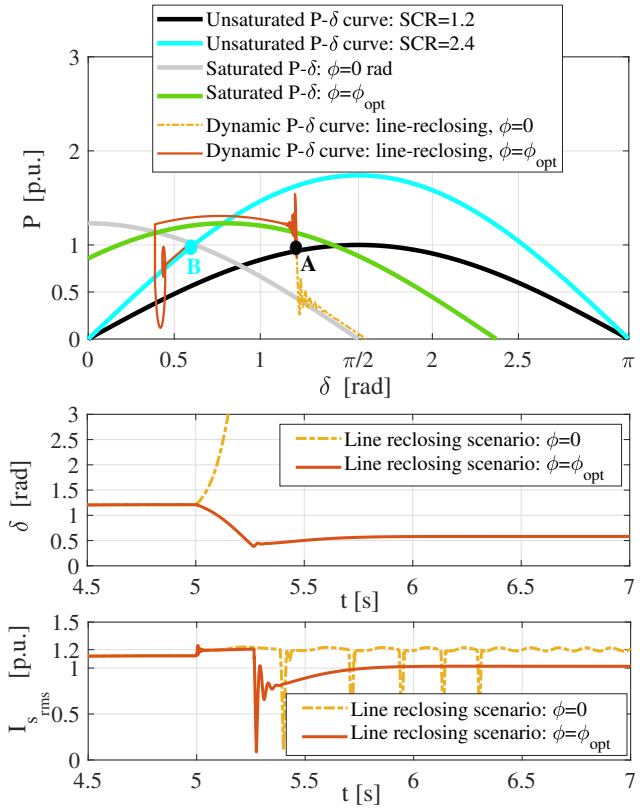

Fig. 15. Dynamic simulation of the line-reclosing under low SCR.

mode, a new degree of freedom is identified, which is the angle of the saturated current reference. Thanks to the derived formulas for the critical clearing angle and critical clearing time in case of a voltage sag event, the impact of this angle on the transient stability has been investigated and its optimal value has been designed. It was also demonstrated that this optimal value enhances the stability margin in case of a phase shift event. It has been demonstrated that this angle has a major positive effect in the case a phase shift than for voltage sag. This is explained by the fact that the proposed method does not prevent the power angle deviation caused by the power mismatch in the power control loop. Therefore, a combination of the proposed solution with an additional transient active power management would result in higher system performances. In the future works, more focus can be made on the dynamic management of the the proposed control degree of freedom. Moreover, it is worthy to compare the effect of using different current limiting strategies (i.e. current saturation algorithm and virtual impedance) on transient stability in case of various grid events.

ACKNOWLEDGMENT

This work is supported by the project "HVDC Inertia Provision" (HVDC Pro), financed by the ENERGIX program of the Research Council of Norway (RCN) with project number 268053/E2, and the industry partners; Statnett, Statoil, RTE and ELIA.

REFERENCES

[1] E. Rokrok, M. Shafie-khah, and J. P. S. Catalão, "Review of primary voltage and frequency control methods for inverter-based islanded microgrids with distributed generation," *Renew. Sustain. Energy Rev.*, vol. 82, pp. 3225–3235, 2018.
[2] European Union, "Commission Regulation (Eu) 2016/631," *Off. J. Eur. Union*, no. 14 April 2016, p. 68, 2016.
[3] A. Adib, B. Mirafzal, X. Wang, and R. Blaabjerg, "On stability of voltage source inverters in weak grids," *IEEE Access*, vol. 6, pp. 4427–4439, Jan. 2018.
[4] A. Ulbig, T. S. Borsche, and G. Andersson, "Impact of low rotational inertia on power system stability and operation," in *19th IFAC World Congress*, 2014, pp. 7290–7297.
[5] I. Sadeghkhani, M. E. H. Golshan, J. M. Guerrero, and A. Mehrizi-Sani,"A Current Limiting Strategy to Improve Fault Ride-Through of Inverter Interfaced Autonomous Microgrids," *IEEE Trans. Smart Grid*, vol. 8, no. 5, pp. 2138–2148, Sep. 2017.
[6] G. Denis, T. Prevost, M.-S. Debry, F. Xavier, X. Guillaud, and A. Menze, "The Migrate project: the challenges of operating a transmission grid with only inverter-based generation. A grid-forming control improvement with transient current-limiting control," *IET Renew. Power Gener.*, vol. 12, no. 5, pp. 523–529, 2018.
[7] L. Huang, H. Xin, Z. Wang, L. Zhang, K. Wu, and J. Hu, "Transient Stability Analysis and Control Design of Droop-Controlled Voltage Source Converters Considering Current Limitation," in *IEEE Trans. Smart Grid*, vol. 10, no. 1, pp. 578–591, Sep. 2017.
[8] A. D. Paquette and D. M. Divan, "Virtual Impedance Current Limiting for Inverters in Microgrids With Synchronous Generators," *IEEE Trans. Ind. Appl.*, vol. 51, no. 2, pp. 1630–1638, Mar. 2015.
[9] T. Qoria et al, "Tuning of AC voltage-controlled VSC based linear quadratic regulation," in *IEEE Milan PowerTech*, 2019.
[10] T. Qoria, F. Gruson, F. Colas, X. Kestelyn, and X. Guillaud, "Current limiting algorithms and transient stability analysis of grid-forming VSCs," *Electr. Power Syst. Res.*, vol. 189, p. 106726, Dec. 2020.
[11] H. Wu and X. Wang, "Design-oriented transient stability analysis of grid-connected converters with power synchronization control," *IEEE Trans. Ind. Electron.*, vol. 66, no. 8, pp. 6473–6482, Aug. 2019.
[12] D. Pan, X. Wang, F. Liu, and R. Shi, "Transient Stability of Voltage-Source Converters with Grid-Forming Control: A Design-Oriented Study," *IEEE J. Emerg. Sel. Top. Power Electron.*, vol. 8, no. 2, pp. 1019–1033, Jun. 2020.
[13] Z. Shuai, C. Shen, X. Liu, Z. Li, and Z. John Shen, "Transient angle stability of virtual synchronous generators using Lyapunov's direct method," *IEEE Trans. Smart Grid*, vol. 10, no. 4, pp. 4648–4661, 2019.
[14] T. Qoria, F. Gruson, F. Colas, G. Denis, T. Prevost, and X. Guillaud, "Critical clearing time determination and enhancement of grid-forming converters embedding virtual impedance as current limitation algorithm," *IEEE J. Emerg. Sel. Top. Power Electron.*, vol. 8, no. 2, pp. 1050–1061, Jun. 2020.
[15] T. Qoria, E. Rokrok, A. Bruyere, B. Francois, and X. Guillaud, "A PLL-Free Grid-Forming Control with Decoupled Functionalities for High-Power Transmission System Applications," *IEEE Access*, vol. 8, pp. 197363–197378, Oct. 2019.
[16] T. Qoria, "Grid-forming control to achieve a 100% power electronics interfaced power transmission systems," PhD thesis, HESAM Université, Nov. 2020.
[17] H. Xin, L. Huang, L. Zhang, Z. Wang, and J. Hu, "Synchronous Instability Mechanism of P-f Droop-Controlled Voltage Source Converter Caused by Current Saturation," *IEEE Trans. Power Syst.*, vol. 31, no. 6, pp. 5206–5207, Nov. 2016.
[18] H. Yuan, X. Yuan, and J. Hu, "Modeling of Grid-Connected VSCs for Power System Small-Signal Stability Analysis in DC-Link Voltage Control Timescale," *IEEE Trans. Power Syst.*, vol. 32, no. 5, pp. 3981–3991, Sep. 2017.
[19] P. Kundur, N. Balu, and M. Lauby, *Power system stability and control.*, New York: McGraw-hill, 1994.
[20] S. Liemann, T. Hennig, L. Robitzky, C. Rehtanz, and M. Finkelmann, "Analysis of the stability and dynamic responses of converter-based generation in case of system splits," *IET Gener. Transm. Distrib.*, vol. 13, no. 16, pp. 3696–3703, 2019.